metals

MDPI

Article

A Methodology to Evaluate the Reliability Impact of the Replacement of Welded Components by Additive Manufacturing Spare Parts

Armando Coro [1,2], Luis María Macareno [1,*], Josu Aguirrebeitia [1] and Luis Norberto López de Lacalle [1]

[1] Department of Mechanical Engineering, Faculty of Engineering in Bilbao, University of the Basque Country UPV/EHU, Paseo Rafael Moreno "Pitxitxi", #3, 48013 Bilbao, Spain
[2] Department of Mechanical Technology, Industria de Turbo Propulsores, S.A.U, Parque Tecnológico, #300, 48013 Zamudio (Bizkaia), Spain
* Correspondence: luismaria.macareno@ehu.eus; Tel.: +34-94-601-4378

Received: 17 July 2019; Accepted: 22 August 2019; Published: 26 August 2019

Abstract: This article shows a method for inspection scheduling of structures made by additive manufacturing, derived from reliability function evaluations and overhaul inspection findings. The routine was an adaption of an existing method developed by the authors for welded components; in this latter case, the routine used a stochastic defect-propagation analysis for pores and lack of fusion defects of additive manufacturing process, instead of the weld liquation crack. In addition, the authors modified the specific stress-intensity factor for welded components to consider additive manufacturing-related material property variability, defect distributions, flaw-inspection capabilities, and component geometry. The proposed routine evaluated the failure rate and inspection intervals using the first-order reliability method (FORM + Fracture) to alleviate the computational cost of probabilistic defect-propagation analysis. The proposed method is one of the first applying reliability concepts to additive manufacturing (AM) components. This is an important milestone, since in 10 years, additive manufacturing is to be used for 30% of the components in aeroengines. This paper presents an example comparing the reliability and cost of a jet engine, with components either made by additive manufacturing or welded parts; in the process, the reliability AM-key features are found, and overhaul schedules of an airplane fleet made with AM components are defined. The simplicity and performance demonstrated in the comparison make the proposed method a powerful engineering tool for additive manufacturing assessment in aeronautics.

Keywords: fracture modeling and simulation; fatigue fractures; manufacturing defects; additive manufacturing

1. Introduction

Aeronautics, in the special aeroengine subsector, is pushing hard to introduce powder bed 3D additive manufacturing (AM) because, with an optimal design, weight savings greater than 20% can be achieved in some cases [1]. Inconel 718 used for aeroengine components is easy to cast but difficult to machine. Therefore, the AM technology is a great candidate for future designs. However, in the process, pores can appear if printing parameters are not fine-tuned. Figure 1 shows some defects and pores due to lack of filling in layer-crossings, in this case, applying 67° between successive layers. The resolution of Digital X-Ray inspection cabins is usually not enough to detect pores, but it detects voids. Up to date, there is only a few works giving some values of probability of defects [2–5] and in many cases, in structural lattice made on purpose.

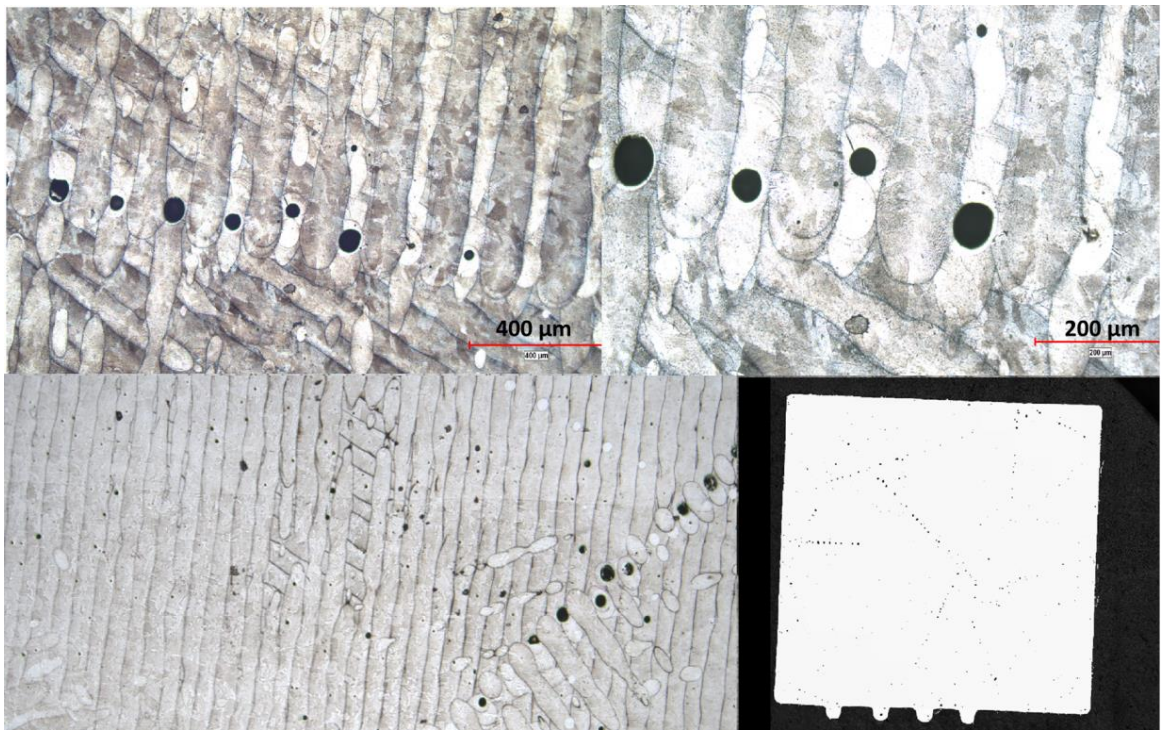

Figure 1. Porosity in SLMed parts: details of rows of pores and test part (200 × 200 mm^2).

AM allows the replacement of various components welded and joined by just one single part [6,7]. Therefore, the AM technology eliminates the need of having large spare warehouses but it requires an additional reliability evaluation to update the failure rate and inspection intervals of the spare components. AM-components may contain undetected defects, because the non-destructive-testing methods available as UT [8] and X-Ray computed tomography [5,9,10] (used in Figure 1) are not fully effective to detect AM lack of fusion [10,11] and AM porosity defects [3,4,12]. Those defects can lead to unexpected component fracture and unscheduled replacement.

In additive SLM parts, all topics related to the influence of defects and surface quality are still under study. Some studies [13–15] define coefficients to be applied in several surfaces affected by laser power and polishing; other works [16] aimed at building orientation, heat treatment, surface quality, energy density, and service condition of the final product in steel SLMed components. Surface state was and it will be key in fatigue.

This paper develops a new probabilistic-fatigue-analysis method for AM-components, which follows the methodology used for welded structures explained by Coro et al. in [17]. The methods applied in [18–56], based in damage-tolerance analysis, wouldn't consider any component coming from additive manufacturing.

The present approach suggests the possibility that several components are manufactured by the so-called powder-bed printing technique in Inconel 718; the methods developed in previous work by the authors [17] for reliability updating, are upgraded now to include the AM design parameters, inspection methods, and component-loading conditions. The improved method incorporates a specific AM defect stress-intensity factor, and several specific AM volumetric probability-distribution-function (PDF): one for defects (pores or lack of fusion), another for inspection results (cracks), and the last for component stress. The proposed routine achieves a required reliability target, with minimum inspection and manufacturing cost for an AM-component.

The paper is structured as in [17], and it is established upon the flowchart in Figure 2, showing four loops that can be replayed separately or simultaneously during all of the AM-component life phases. The process is similar to the one presented in [17], but with several substantial differences, highlighted in the following paragraphs.

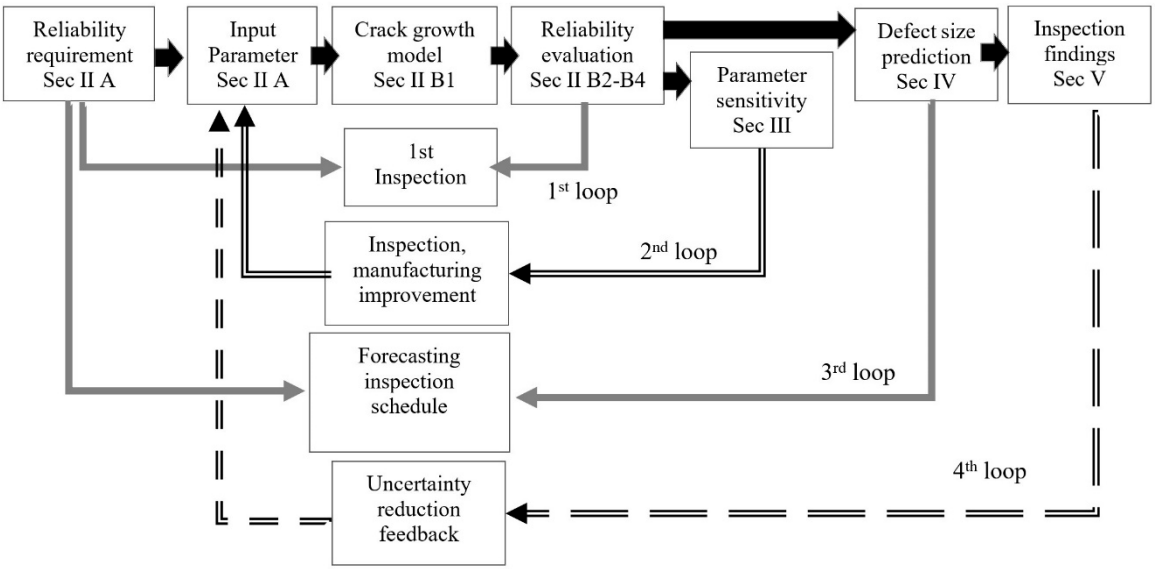

Figure 2. Proposed steps in the additive manufacturing (AM)-component reliability-evaluation method.

The first loop, mandatory in the AM-component design process, defines the first inspection based on a required target reliability. As a first step, the AM-component target reliability is the same that the one of the welded-component by which is replaced, the weld concentration factor and angular misalignment parameters are removed, and the AM-component defect distribution is redefined by a volumetric distribution, as explained in Section 2.1.1. In addition, the defect-growth laws are modified to remove the welded part geometrical characteristics, and the crack aspect ratio consideration is modified (as described in Section 2.1.2). Finally, the reliability evaluation is performed in the same manner, and a comparison of this output with the required target reliability defines a first inspection schedule, and a comparison with the welded-component to replace.

The second loop remains the same; it is a sensitivity analysis of the manufacturing route of the AM-components. The AM-parameters and the defect-growth laws are used as input data, to evaluate the reliability and the parameter sensitivity study, as described in Section 2.2. The results allow the definition of a new set of AM-parameters, the improvement of the inspections methods (to include the X-Ray computed tomography [5,9,10] and ultrasonic testing (UT) [8]), and the modification of the manufacturing route (to include Hot Isostatic Pressure (HYP) [57,58], annealed [10]). The new AM-parameters can be used as feedback to replay the first loop or to redefine the inspection schedule.

The third loop corresponds to the update of a reliability estimate after each inspection. Again, the AM-parameters are the input data. A unique AM parameter a_i, that defines simultaneously the defect rate and size found during inspection is forecasted as explained in Section 2.3 (in contrast, a welded-component needs two separate parameters to define the defect size a_i and rate δ). Finally, the reliability evaluation is forecasted based on the removal of defective parts after each inspection, which provides a well-known saw-tooth reliability graph.

The fourth loop focus on the service-support process of AM-component. An AM-component has more undetectable defects than a welded-component. In addition, the AM-component has smaller defect size, and then a component testing is needed because of the reduced inspection effectiveness in the beginning of the component life. At this stage, the defect size evaluated in loop 3 (Section 2.3) is compared with the inspection findings (Section 2.4). Thus, by using the maximum likelihood analysis, the AM-parameters can be updated, and loops 1, 2 and/or 3 can be replayed to achieve an "Inspection scheduling based on reliability updating for AM-components".

As outlined in the previous paragraphs, the paper highlights the novelties of the methodology in order to be applied in AM components, taking as baseline the method developed for welded components. Sections 2.1 and 2.2 explain the damage-growth model, which originally incorporate the

AM-component parameters as volumetric defect size, finding size, and stress probabilistic distribution. In addition, it contains the defect-growth model, that incorporates a specific SIF for AM pores and lack of fusion defects in an AM-plate, and the innovative reliability estimation method, that uses FORM + fracture method in AM component. Section 2.3 explains the process to evaluate and forecast the reliability after each inspection, which uses FORM method in AM component. Section 2.4 explains the method to predict inspection findings, and an innovative FWMSV maximum-likelihood-estimator methodology to update the defect-growth model considered. Section 3 compares the numerical example of a pressure-containment case reported in [17], and manufactured by electron-beam welding process, with the same component manufactured by power bed 3D AM. Section 4 contains the main conclusions of the work.

2. Methodology

2.1. Loop 1: Reliability Evaluation and First Inspection Schedule

2.1.1. Inputs: Target Reliability and Additive Manufacturing Parameters

The replacement of welded-components by additive manufacturing spare parts is possible if the required target-reliability (defined as failure probability during the N load cycles) is fulfilled, and inspection schedule is maintained.

Besides, the AM-parameters (AM defect-growth variables) must be considered as statistical input variables [29]. Most of the parameters are similar to a welded-component, and they are grouped in different categories, as for a welded-component, as shown in Table 1.

Table 1. Additive manufacturing parameters.

Parameter Group	Parameter	Units	Description
Inspections	a_i	mm	Half of a surface-flaw initial size
	a_f	mm	Half of a surface-flaw size that triggers component fracture
Material Properties	n	-	Paris–Erdogan equation constants
	c	(mm/cycles)/(MPa^n·m$^{-n/2}$)	
	K_{Ic}	MPa m$^{1/2}$	Material fracture toughness
AM Geometry Acceptance Criteria	t_w	mm	AM-component real thickness
	e	-	AM geometry misalignment (percentage of thickness)
Loads and FEM	σa	MPa	AM-component axial mean stress
	σb	MPa	AM-component bending surface stress
	N	-	Number of load cycles
Method Uncertainty	λ_w	-	Thickness correction-factor for surface-crack stress
	θ	-	Elliptical integral correction-factor for surface-crack stress

The main differences between AM and weld parameters are caused by the defect distribution: the welded-component defect distribution is linear (defects per weld length mm) and the AM-component is volumetric (defects per AM-component volume mm^3). If the component under evaluation is split into several analysis areas [34] with a constant dimension, then, the AM-component analysis requirements would be roughly equal to the analysis requirements of the welded components raised to the cube, and the computational cost will increase in the same amount. In this sense, the AM-parameters in Table 1 are modified to consider a unique analysis area, allowing a reduction of the computational cost of a reliability evaluation.

(1) Inspections

For a welded-component the a_i parameter considers the findings size and the probability of detection (POD) of the finding, and the δ parameter considers the number of findings [17]. The AM-component uses the same a_i parameter of a welded-component, but with a different meaning; the AM pores and lack of fusion defects occurrences per unit of volume δ variable is taken into account within the a_i parameter. The probability-distribution-function (PDF) a_i is evaluated based on the cut-ups of AM-parts, and it considers the findings size, number, and POD.

Besides, the final surface defect size a_f prior to failure is fully correlated with the K_{Ic} (fracture toughness) statistical input variable, which is one of the AM material properties defined in the next section.

(2) AM material properties

The AM component uses the same parameter descriptions of the welded-component, The AM pores and lack of fusion defects are considered sharp cracks, and they grow according to the rates defined by the Paris–Erdogan equation parameters c and n [21]. Fracture (failure) happens when the defect size reaches K_{Ic} (fracture toughness), with a specific final defect size a_f [36,37]. The proposed methodology considers negligible the AM-component anisotropy [59], defect-growth threshold, residual stresses, and defect-growth retardation effect due to compressive loads.

(3) AM geometry acceptance criteria

The stress concentration factor of weld and the angular misalignment acceptance criteria are not considered in the case of the AM-component. The geometry acceptance criteria restrict the AM geometry misalignment e, and the thickness variation t_w [39]. The AM process is not acceptable until t_w and e parameters are below allowable limits. The variables have an independent PDF, with a mean value that agree with the AM-components nominal dimensions, and standard deviations that correspond to the AM acceptance limits.

(4) Loads and finite-element method

The load is defined by the load repetition times N and two independent statistical variables, the AM-component axial stress σ_a and the AM-component bending stress σ_b. Both are gotten from a flawless AM-component finite-element model (FEM). The AM-component uses the same parameter descriptions of a weld component, but with a different meaning. The σ_a and σ_b weld parameters mean values correspond to mean stress in the different analysis areas, and the standard deviation values correspond to the uncertainty. On the other hand, the σ_a and σ_b AM parameters mean and standard deviation correspond to the stress distribution in the AM-component and load uncertainty, at the same time.

(5) Method uncertainty

The AM-component uses the same parameter descriptions of the welded-component explained in [17]. Variables λ_w and θ correspond to the statistical scatter in stress-intensity factor (SIF) between the proposed routine and the complex 3D cracked AM-component FEM (most realistic crack growths possible evaluation).

2.1.2. Method: Probabilistic Damage-Growth Model for AM-Components

(1) Defect-Growth Model

The paper uses a defect-growth model similar to that explained in [17] (Equations (1)–(7)). It is applicable for plates and welded plates, and it is based on mode I Paris-Erdogan [21] propagation law

(Equation (1)) of a surface elliptical crack in a plate, which calculates the SIF as a function of the axial and bending loads [41], as shown in Equation (2).

$$\frac{da}{dN} = c \cdot \Delta K(a)^n \tag{1}$$

$$\Delta K(a) = \frac{1}{1.57} \cdot \left(\left(1.119 + 0.431 \cdot \frac{a}{t}\right) \cdot \sigma a + 1.076 \cdot \sigma b\right) \cdot \sqrt{\pi \cdot a} \tag{2}$$

Two modifications are considered to adapt the defect-growth model to AM components. First, two weld specific parameters are removed: the welding concentration factor, avoiding Equation (6) in [17], and angular misalignment, replacing the Equation (5) in [17] by Equation (3) below. Both parameters increase the defect-growth rate; the concentration factor increases the SIF and the angular misalignment increase the bending stress to consider. Both are not necessary in the case of an AM component, because the AM geometry avoid any unnecessary concentration factor, and the AM manufacturing reduces considerably the angular misalignment. Only, the AM-component thickness t_w, and misalignment e update the axial and bending stresses.

Second, the crack dimensions correspond to porosity void in the AM-part surface that have not been removed by HYP process, or to a lack of fusion defect in the high stressed area of the AM-part, instead of a weld liquation crack. During AM-component defect growth, a constant factor of 0.5 between the crack depth and length is considered, instead of the 0.563 welded-component relationship.

$$\sigma b_w = \left(\frac{t_w}{t}\right)^2 \cdot \left(\sigma b + \sigma a \cdot \left(\frac{t_w}{t}\right) \cdot 3e\right) \tag{3}$$

(2) Fracture-Limit and Fatigue-Limit State Function

This paper uses the same fracture and fatigue state functions (FE2 Equation (4)) explained by Coro et al. in [17]. In contrast with welds, the Paris–Erdogan equation integral, Equation (4), is determined by calculating elementary functions. It is possible because the variable change $a = t^2$ fulfill the binomial integration requirements [48]: n is an integer. In summary, the Equations (10)–(12) in [17] are replaced by Equations (5)–(7) bellow.

$$FE2(N,a) = \frac{\int_{ai}^{a} \frac{da}{c \cdot \Delta Kw(a)^n}}{N} - 1 \tag{4}$$

$$\int_{a_i}^{a} \frac{da}{c \cdot (\Delta K_w)^n} = \int_{a_i}^{a} a^{\frac{-n}{2}} \cdot (c_0 + c_1 \cdot a)^{-n} \cdot da \tag{5}$$

$$c_o = \frac{\sqrt{\pi} \cdot c^{\frac{1}{n}}}{1.57} \cdot (1.119 \cdot \sigma a_w + 1.076 \cdot \sigma b_w) \tag{6}$$

$$c_1 = \frac{\sqrt{\pi} \cdot c^{\frac{1}{n}}}{1.57} \cdot \left(\left(\frac{0.431}{t}\right) \cdot \sigma a_w\right) \tag{7}$$

(3) Fracture Probability: FORM + Fracture

This article uses the FORM + fracture method, as explained in [17]. The reliability index β_{fi} in Equation (8) [51] is obtained by an iterative algorithm. It represents the minimum distance between the nominal design and fracture condition in a normalized parameters space. This minimum distance corresponds to the number of standard deviations, and it determines the failure probability.

The AM-component is considered as a single area ($na = 1$), it has always a unique defect because the initial defect size a_i parameter considers the defect occurrence probability per unit of volume δ.

$$\beta_{fi} = \min \sqrt{(x-\mu)^T \cdot C^{-1} \cdot (x-\mu)} \tag{8}$$

2.2. Loop 2: Sensitivity of AM Design Parameters

This article uses the reliability index β sensitivity Equations (17) and (18) in reference [17]. Once the reliability index β has been obtained in loop 1 (see Figure 1), the loop 2 does a sensitivity study of AM parameters to find the most critical ones. The reliability sensitivity to mean and standard deviation of the AM parameters is obtained as a function of the reliability index β, as shown in Equations (9) and (10).

$$\frac{\partial \beta_{fi}}{\partial \mu_j} \approx \alpha_j \tag{9}$$

$$\frac{\partial \beta_{fi}}{\partial \sigma_j} \approx -\beta \cdot {\alpha_j}^2 \tag{10}$$

2.3. Loop 3: Reliability Evaluation after Inspection for AM-Components

This article uses the FORM method, as explained in [17]. The AM-component considers a single area ($na = 1$), and the AM-component defects-size a_d links the defects-size and defect-rate forecasting of the inspection, avoiding the defect rate Equations (20) and (21) in [17].

2.4. Loop 4: Update by Inspection Findings the Probabilistic Damage Growth Model

This article uses the failure-weighted mean-square value (FWMSV) approach, as in [17]. The component inspection findings redefine the inspection plan. The process modifies the AM parameters in Table 1 to minimize the mean square difference value of the crack size exceedance probability weight by the failure probability when that crack size is detected Equation (11).

As explained in Figure 2, once the loop 1 determined the first inspection interval and the loop 3 updated the reliability evaluation, the loop 4 compares the real inspection findings with the flaw size forecasted in loop 3, and updates the AM-component parameters.

$$\mathrm{FWMSV} = \sum_{\mathrm{i}=1}^{\mathrm{nf}} Pf_w(\mathrm{a_i}) \cdot \left(\frac{\mathrm{P}_{ins}(\mathrm{a_i}, \mathrm{N_i}) - \mathrm{P}(\mathrm{a_i}, \mathrm{N_i})}{\mathrm{P}_{ins}(\mathrm{a_i}, \mathrm{N_i})} \right)^2 \tag{11}$$

3. Results and Discussion

This section presents a numerical example to evaluate the reliability of an AM jet engine case based on the developed methodology by Coro et al. in [17]. The example allows the comparison between AM-component and electron-beam welded-components because the load and dimensions are the same that the electron-beam weld case reported in [17]. The evaluated geometry corresponds to an AM cylindrical case of 500 mm height, 707 mm diameter, and 2.2 mm thickness (see Figure 3) of a nickel-based alloy. The loads are generated by the temperature gradient between the atmosphere and the jet engine during a flight cycle. Each flight has a single load cycle, which gets null load at the beginning and maximum stress level at take-off. Skin loads are distributed in 36-mm lengths, with 60 MPa inside and 100 MPa outside the AM cylindrical case, and as seen in Figure 4, they follow a parabolic stress distribution circumferentially.

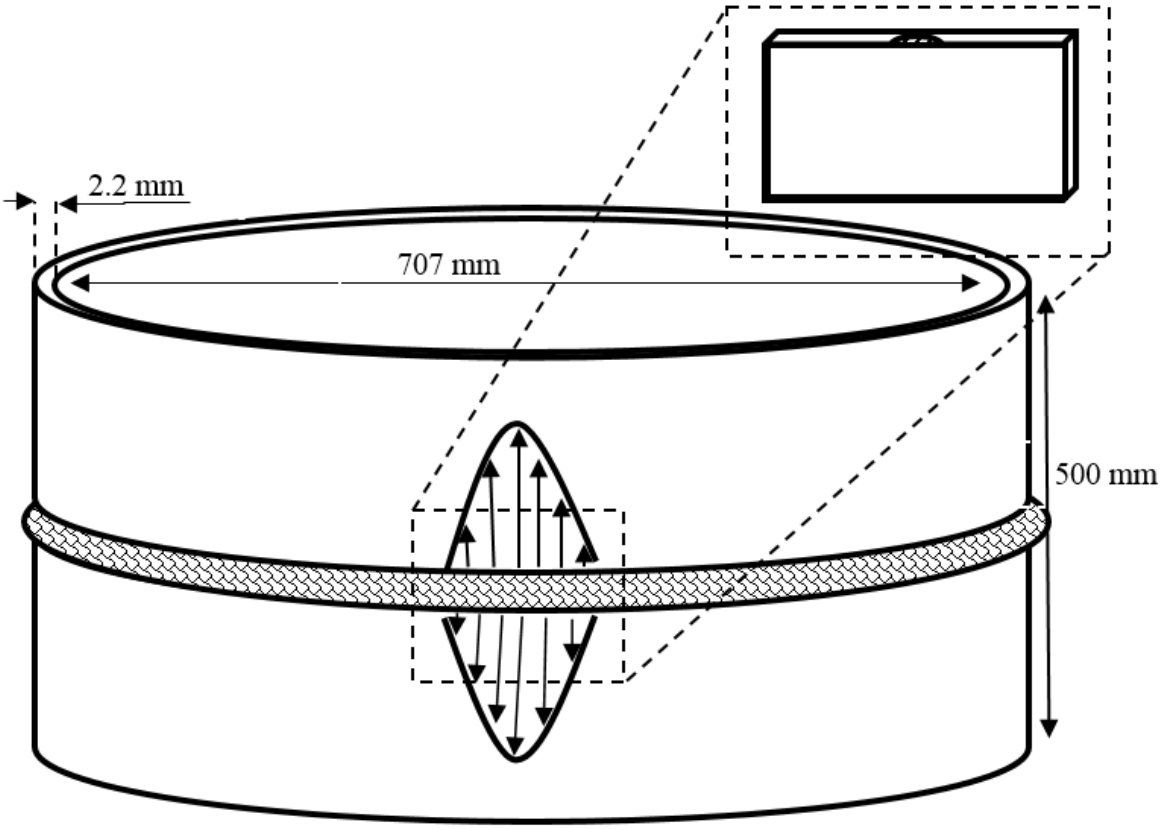

Figure 3. Jet engine AM case.

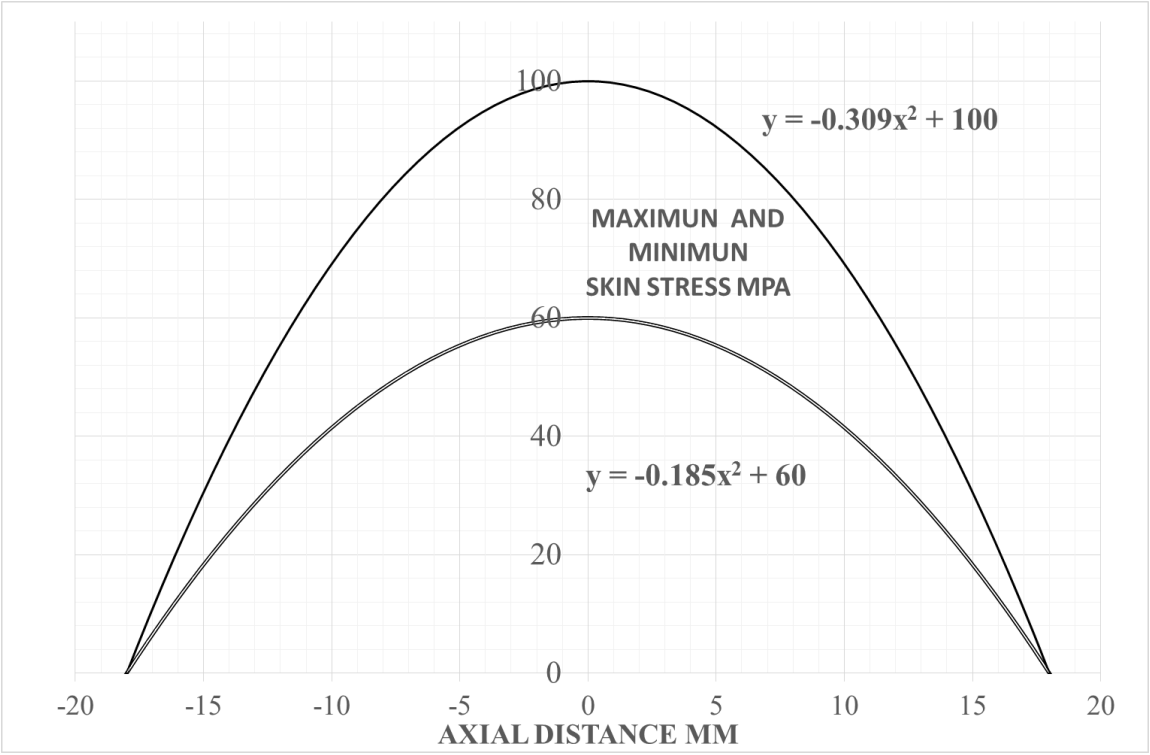

Figure 4. AM cylindrical case circumferential skin stress distribution MPa.

The PDF (mean and standard deviation values) of the parameters considered in the AM-case calculation are summarized in Table 2. The unique AM-component area has a resultant a_i PDF mean

value of 150 µm and a PDF standard deviation of 20 µm. They have been evaluated by the evaluation of AM component cut-ups. The AM-case volume under stress is 39,600 mm^3 ($2.2 \times 36 \times 500$), and it has the same amount of defects per unit of volume as the reference [2], that reports an a_i PDF mean value of 20 µm and a PDF standard deviation of 30 µm in a volume of 0.325 mm^3.

Table 2. AM-case PDF parameters considered in the example.

Parameter Group	Parameter	Units	Mean Value	Standard Deviation	Probability-Distribution Function
Inspections	a_i	mm	0.150	0.02	Normal
	a_f	mm	-	-	-
Material Properties	n	-	3.0	-	-
	c	(mm/cycles)/(MPa^n·m$^{-n/2}$)	2.562×10^{-5}	5.636×10^{-6} (22%)	Lognormal
	K_{Ic}	MPa $m^{1/2}$	5.417	0.5417 (15%)	Normal
AM Geometry Acceptance Criteria	t_w	mm	2.2	0.132 (6%)	Normal
	e	-	0	0.132 (6%)	Normal
Loads and FEM	σa	MPa	18.3	1.7 (11%)	Normal
	σb	MPa	73.3	6.7 (9%)	Normal
	N	-	300	-	-
Method Uncertainty	λ_w	-	1.076	0.054 (5%)	Normal
	θ	-	1.429	0.07 (5%)	Normal

The stresses σ_a and σ_b agree with stress occurrence per unit of volume shown in Figures 3 and 4. They have been evaluated by FEM statistical stress distribution. The geometry acceptance criterion restricts the thickness reduction and misalignment to 6%, and it depends of the AM manufacturing parameters and the rejections requirement. In addition, the defect POD has a PDF mean value of ln(0.38) mm with a PDF standard deviation of 0.677 mm [56]. The POD curves are defined in the industrial NDT standards, or after a statistical hit-miss analysis of a test component inspection finding.

The Paris constant c incorporates the defect-growth variability, and the Paris constant n has a constant value of 3.0. The fracture toughness K_{Ic} accounts the scatter of the final flaw size before failure. Both parameters have been obtained by standard test method to measurement fracture-toughness and fatigue [36,37]. As discussed in Section 2.1.1, the effect of the AM-components anisotropy [59], defect-growth threshold, residual stresses, and defect-growth retardation effect due to compressive loads, are considered negligible during the fatigue-crack growth evaluation.

It is considered that AM-case thickness tolerance is the double of welded-case one and the AM-case method uncertainties are a half of those in the welded-case because of the removal of the weld-stress concentration-factor (AM avoids weld root and crown geometry).

The AM case failure probability target is 1.4×10^{-4} during the first 300 flight cycles, the same that the welded component reliability requirement to replace [17]. A single defect-propagation analysis, which considers the PDF mean value of the parameters in Table 2, predicts a structural fracture of the AM-case at 2152 load cycles.

3.1. Loop 1: AM-Case Probabilistic Damage-Tolerance Assessment

Table 3 shows the failure probability of AM-component vs weld component [17] at 300 load cycles, and the evaluations are replayed at different load cycles to graph the failure-probability shown in Figure 5. The AM-component has smaller defect size and more undetectable defects than a welded-component, and then the AM-Case has a lower fracture probability at the beginning of the AM-component life and a higher fracture probability at the end of the AM-component life.

Table 3. Am-case fracture probability at the end of the service life (300 load cycles).

Component	Maximum Stress, MPa	Equivalent Length, mm	Reliability Index	Crack Probability per Unit of Length	Fracture Probability Worst Location	Failure Probability
AM	100.0	-	3.368	-	3.78×10^{-4}	3.78×10^{-4}
Weld	100.0	17.34	0.5274	5.00×10^{-5}	2.99×10^{-1}	2.59×10^{-4}

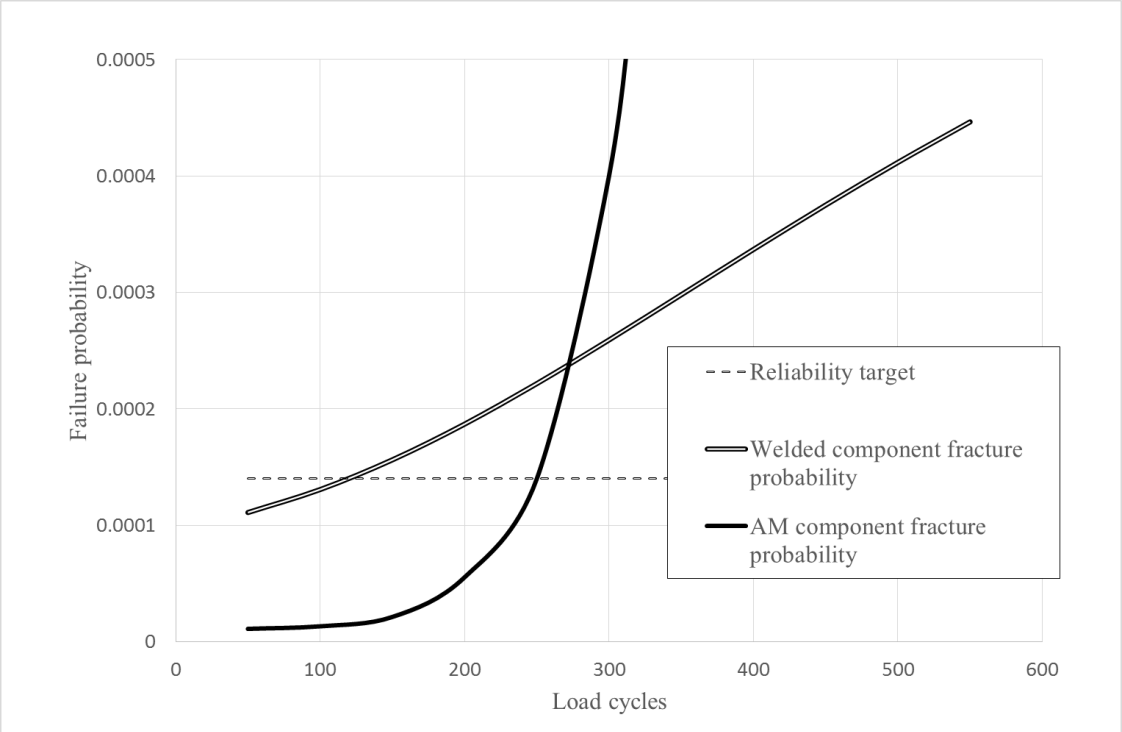

Figure 5. Failure probability without inspection.

In addition, the reliability evaluation of AM-component requires a component testing because of the reduced inspection effectiveness in the beginning of the component life. The AM-case fracture probability overtakes the failure-target at two hundred fifty load cycles, and an overhaul becomes necessary to fix or remove the defective AM-cases.

3.2. Loop 2: AM Parameter Sensitivity

The twelve AM parameters are sorted into five areas of improvement: AM-case inspection, AM-case material properties, AM-case geometry acceptance criteria, AM-case loads, and defect-growth method uncertainty. The PDF mean values in Table 2 are used as a unit reference to obtain the PDF mean and standard-deviation sensitivity values. The linear misalignment (0 value in Table 2) is a special case and it considers the AM-case thickness t as a unit reference.

Table 4 shows the (reliability index) β_{fi} sensitivity of the AM-case, using Equations (17) and (18) in [17]. Figure 6 has been obtained by adding the sensitivities of the parameters in each area of improvement (Table 4), and it shows the guidelines to upgrade the AM-component reliability in a new component design. First, the "AM geometry acceptance criteria" have a 31% and 43% of the contribution; It is the focus area to improve the AM-case reliability. Second, the "AM initial crack size" has only 7% and 4% of the contribution; them the non-destructive test inspection process proposed for the AM-case could be reduced. Third, the "AM material properties" and "loads and FEM" show a medium contribution on the reliability with 22% and 18% effect respectability. Finally,

the "defect-growth method-uncertainty" gives a 21% and 17% upgrade. If 3D FEM modelling refines the calculations, the reliability index improvement could reach 20%.

Table 4. AM-case PDF parameters reliability-index sensitivity.

Parameter Group	Relevant Parameter	Mean-Value Sensitivity	Standard-Deviation-Value Sensitivity
Inspections	a_i	0.203	−0.139
	a_f	-	-
Material Properties	n	-	-
	c	0.271	−0.247
	K_{Ic}	−0.333	0.373
AM Geometry Acceptance Criteria	t_w	0.617	−1.282
	e	0.23	−0.178
Loads and FEM	σa	0.123	−0.051
	σb	−0.4	0.539
	N	-	-
Method Uncertainty	λ_w	−0.326	0.358
	θ	0.245	−0.202

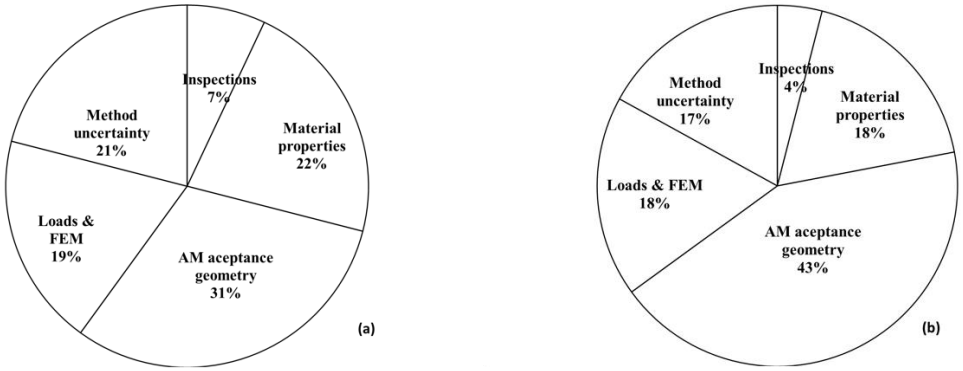

Figure 6. Parameters weight in AM-component reliability. PDF mean (**a**) and standard deviation (**b**) values.

The (reliability index) β_{fi} sensitivity is completely different between AM-case and welded-case, because of the initial AM-case anomaly size is a 40% (0.15/0.38) of the welded-case. On the other hand, the acceptance geometry is the main parameter to focus on AM-case, and material properties in welded-case, because the AM material have a lower n Paris-Erdogan equation constant than welded material.

3.3. Loop 3 Parts 1 and 2: AM-Case Inspection-Finding Prediction

The proposed procedure is replayed at three different inspection intervals: an unused AM-case at 0 load cycles, at 100 load cycles, and at 200 load cycles. As expected, Table 5 shows that the findings increase with the load cycles. The inspections POD is a lognormal variable PDF mean value of ln(0.38 mm) and PDF standard deviation of 0.677. It is the same POD as that for welded-components considered in [17]. The findings PDF gets a shape similar to a lognormal PDF. The integration of Equation (19) in [17], simulates the inspection, and it gets the 27% of the defective parts, at 100 load cycles. If the inspection is repeated at 200 load cycles, the defective parts found increase to 48%. The AM-case percentage of defects found is similar to the welded-case [17].

Table 5. AM-case percentage findings of defects found.

Inspection at Load Cycles	Percentage of Defects Found (%)
0	0.00%
100	27.60%
200	48.40%

3.4. Loop 3 Part 3: AM-Case Inspection Plan

As shown in Figure 5, when the AM-case failure probability overcome the required failure probability target. Then, two inspection intervals at 100 and 200 load cycles become necessary to remove defective AM-Case.

As explained in Section 3.3, the first inspection at 100 load cycles, decreases the failure probability a 27.6% because of the withdrawal of defective AM-case. The second inspection, at 200 load cycles, decreases the failure rate a 48.4% As shows Figure 7, it is not enough to achieve the reliability target at 300 load cycles.

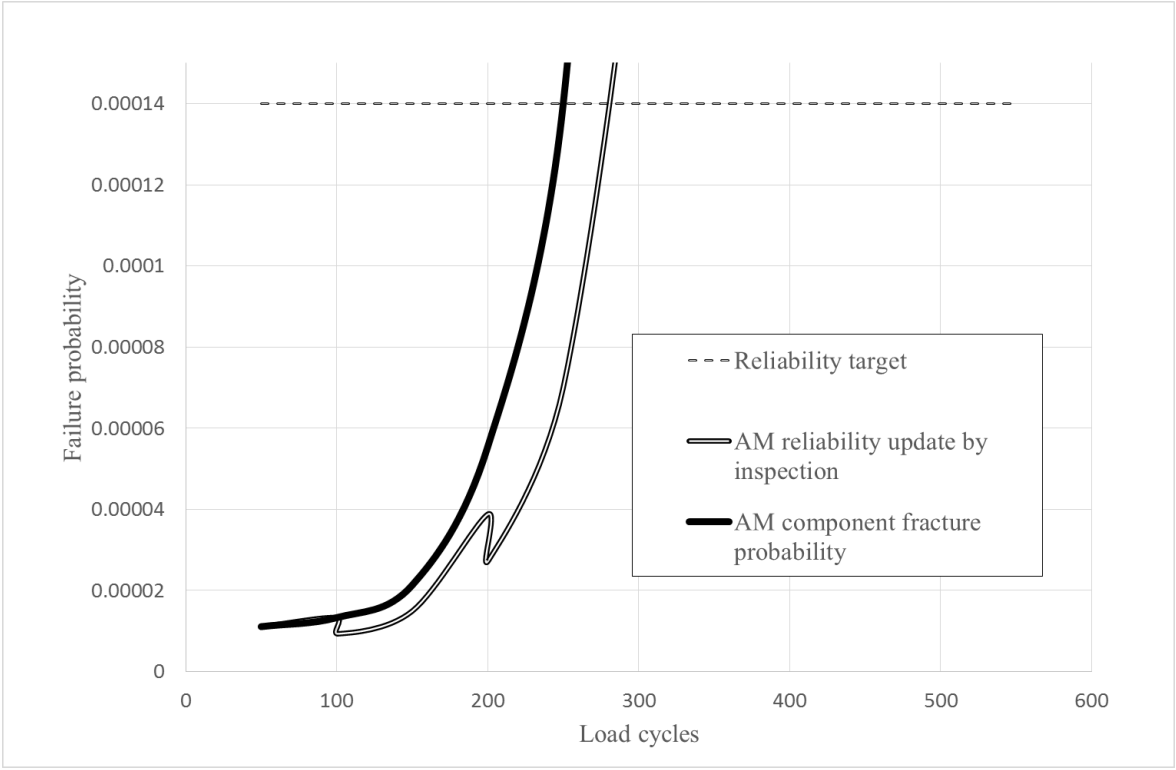

Figure 7. AM-Case failure probability with inspection.

The AM-case failure probability increases exponentially at 200 cycles, in contrast, the welded-case failure probability increases linearly. The failure probability does not reach the reliability target value during component life, and welded-case could not be replaced by an AM-case.

3.5. Loop 4: AM PDF Parameter Update by Inspection Findings

Ten AM-case fracture tests have been considered to improve the reliability. The fracture-defect-size and load cycles reached in the fracture test ("Fleet B" column in Table 6) have been created by the AM-case nominal parameters (Table 2), and a 10% reduction of loads σ_a and σ_b.

Table 6. 10 defect size after a component fracture.

Defect Number	Probability of Fracture Defect-Size Exceedance	"Fleet A"		"Fleet B"	
		Fracture Defect Size (mm)	Load Cycles	Fracture Defect Size (mm)	Load Cycles
1	0.091	1.21	1062	1.493	1516
2	0.182	1.344	1277	1.658	1823
3	0.273	1.473	1506	1.818	2150
4	0.364	1.6	1751	1.975	2500
5	0.455	1.727	2018	2.132	2881
6	0.545	1.856	2312	2.292	3301
7	0.636	1.991	2644	2.459	3776
8	0.727	2.138	3036	2.640	4336
9	0.818	2.31	3540	2.853	5055
10	0.909	2.584	4448	3.192	6352

On the other hand, the fracture-defect-size and load cycles reached in the fracture test ("Fleet A" column in Table 6) have been forecasted by the AM-case nominal parameters

The analysis proposed upgrades the AM-case nominal parameters until the predicted fracture defect size and cycles are close to the ten fracture-defect-size and cycles of the fracture test. Then, the analysis update will reduce the failure probability of the AM-case reported in loop 3, because the forecasted defect size and loads cycles are lower than the fracture test ones.

The Table 2 parameters upgrade is restrained by the uncertainty weight in Table 7. Only AM specific parameters are considered: the AM inspection and AM material properties parameters will be modified during the updating process.

Table 7. Parameters uncertainty weight.

Relevant Parameters Group	Relevant Parameter	Mean-Value Uncertainty	Standard-Deviation Value Uncertainty
Inspections	a_i	1	1
	a_f	-	-
Material Properties	n	-	-
	c	1	1
	K_{Ic}	1	1
AM Geometry Acceptance Criteria	t_w	0	0
	e	0	0
Loads and FEM	σa	0	0
	σb	0	0
	N	-	-
Method Uncertainty	λ_w	0	0
	θ	0	0

As a welded-component, the failure-weighted mean square value (FWMSV) method, explained in Section 2.4, gives a good sensitivity to lead the AM-component "Fleet A" input parameters update and avoid numerical errors. The "Fleet B" FWMSV value of 0.032, reported in Table 8, is a FORM + fracture routine numerical errors estimation. On the other hand, the "Fleet A" FWMSV of 11.664 is 365 times greater than the predicted numerical error of 0.032.

Table 8. Failure-weighted mean-square value (FWMSV) Adjustment evaluation

"Fleet A"	11.664
"Fleet B"	0.032
"Fleet B update"	0.029
Target	0

The inspection update proposed is derived from the "Fleet A" AM-Case input parameters (Table 2) and the findings obtained from "Fleet B" data. As reported in Table 9, a new set of AM-Case parameters, called "Fleet B update", have been obtained.

Table 9. AM-Case parameters update proposal.

Relevant Parameters Group	Relevant Parameter	Mean-Value Update Need	Standard Deviation Value Update Need
Inspections	a_i	0.127 (−15.2%)	0.01997 (−0.2%)
	a_f	-	-
Material Properties	n	-	-
	c	2.037×10^{-5} (−20.5%)	5.40×10^{-6} (−0.2%)
	K_{Ic}	5.94 (9.7%)	0.54 (−0.1%)
Welding Geometry Acceptance Criteria	t_w	-	-
Loads and FEM	σa	-	-
	σb	-	-
	N	-	-
Method Uncertainty	λ_w	-	-
	θ	-	-

The results give three main conclusions: First, the impact of the AM-parameters standard-deviations is minimal. Second, the material-properties c mean value is the key parameter to upgrade the reliability evaluation. Third, the reliability update problem has multiple possible solutions; in this case, the load reduction imposed in "Fleet B." is compensated by the increase in material properties c.

3.6. Repeating Loop 1 after Loop 4: "Fleet B Update" Probabilistic Damage-Tolerance Assessment

AM-case failure probability evolution, during the example steps, is represented in Figure 8. The "Fleet A" fracture-probability curve is the same as that obtained in Section 3.1. The "Fleet B" fracture-probability curve has been obtained after a 10% load reduction. The "AM reliability-update-by-inspection curve" fracture-probability curve has been obtained by the "Fleet A" AM-parameter upgrade, based on the "Fleet B" findings in Section 3.5. As expected, a graph close to the "Fleet B".

As commented in Section 3.5, the analysis update will reduce the failure probability of the AM-case reported in Section 3.4, because the forecasted defect size and loads cycles are lower than the fracture test ones. Then, the reliability target, of a 1.4×10^{-4} rate during AM-Case service life, is fulfilled and the reliability increase enables the elimination of the inspections proposed in Section 3.4 (at 100, and 200 load cycles).

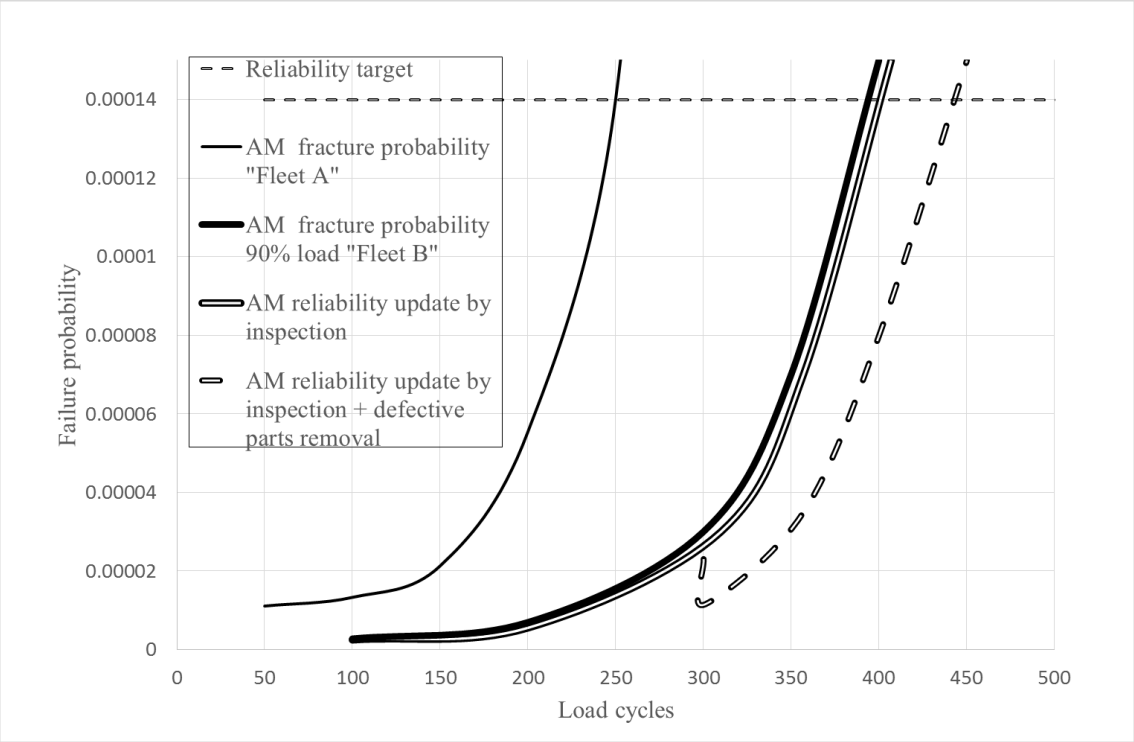

Figure 8. Failure-probability update.

3.7. Repeating Loop 3 after Loop 4: "Fleet B Update" Inspection Update

The AM-case failure probability increases exponentially at 300 cycles, and the reliability target is not fulfilled at 400 load cycles. After an inspection at 300 load cycles, with a defective-part removal percentage of 44%, the reliability requirement is fulfilled at 400 cycles, as shown in Figure 8 ("AM Reliability update + defective parts removal" graph).

4. Conclusions

This paper develops a method for the inspection schedule in AM-components. The methodology is based on a stochastic defect-propagation analysis that improves input parameters to predict the inspection findings. It considers the uncertainty in AM material properties, AM defect-inspection capabilities, defect-growth calculation methods, and loads. The key characteristic of the submitted methodology are:

1. A novel AM defect-growth routine is developed. It incorporates a specific SIF for AM pores and lack of fusion defects in an AM-plate. The formulation proposed allows the use of elementary functions to evaluate the Paris law equation integral, and it considers the main parameters of AM-component reliability (AM inspections capability, AM material properties, loads, AM geometry, and defect-growth method uncertainties). The approach reduces the computing time by 400 times when compared with a reliability evaluation, which uses explicit crack growth analyses and Monte Carlo Simulation (MCS).
2. An AM-component can use the same reliability updated methods as for a welded-component: FORM to forecast the defect growth, FORM + fracture to reliability calculation, and FWMSV finding-size likelihood estimator to update AM-parameters.
3. The AM-component volumetric defect size, finding size, and stress probabilistic distribution functions allow the reliability evaluation with a unique crack propagation analysis, avoiding the component division into different areas, and reducing the computational cost. The approach reduces the computing time by 10 times when compared with the welded component example of 36 mm loaded length [17].

The methodology compares AM-components reliability and economical cost with welded-components, because the parameters are grouped in the same categories as welded-components. The example shows that the AM-component has a lower fracture probability at the beginning of the AM-component life, and a higher fracture probability at the end of the AM-component life than a welded-component. On the other hand, AM-component fracture tests have become necessary because of the AM-component inspections are less effective than welded-component inspections. In addition, the AM component first inspection requirement and defect grow life with nominal AM parameter gives a factor of 8 (2152/250), bigger than 5 (550/125) obtained for welded structure in [17].

Finally, the routine low computational cost (400 times faster) allows the use of the methodology in several areas where stochastic reliability evaluations have not been developed yet. During the replacement of a welded component by an AM one, an effective "design for the manufacturing" practice can be reached. During the service of an AM-component, the structural-health-monitoring application can define a specific replacement for each component by the incorporation of a defect-growth routine that acquires knowledge during the AM-component lifecycle. On the other hand, the method can improve AM-parts replace schedules of an airplane based on fracture test.

Author Contributions: A.C. writing and formal analysis, L.M.M. review and editing, J.A. and L.N.L.d.L. review and technical supervision.

Funding: This research received no external funding.

Acknowledgments: We are thankful to Silvia Martinez, for the valuable SLM data and advices. The invaluable supporting and helping from the Mechanical Technology Department of ITPAero® is recognized with great appreciation.

Conflicts of Interest: The authors declare no conflicts of interest or state.

Abbreviations

a	Elliptical crack semi axis
a_i	Half of a surface anomaly initial size
a_d	Half of a surface anomaly size detected during inspection
a_f	Half of a surface anomaly size that triggers component fracture
c	Paris-Erdogan equation constant
c_0	Stress-intensity factor variable-change constant
c_1	Stress-intensity factor variable-change constant
e	Weld linear misalignment expressed as a percentage of the thickness
n	Paris-Erdogan equation constant
na	Number of studied areas
t	AM-component nominal thickness
t_w	AM-component real thickness
K_{Ic}	Material-fracture toughness
N	Number of load cycles
Pf_{Ai}	Probability of failure
P(N,a)	Probability of have 2a crack after N load cycles (Analytically calculated)
P_{ins}(N,a)	Probability of have 2a crack after N load cycles (Based in inspection findings)
α_i	FE2 Failure surface gradient vector in the weld design parameters space
β_{fi}	Reliability index to reach AM-component fracture
δ	Defect-occurrence probability per unit of AM-component volume
μ_i	AM design parameter mean value vector
σa	Axial mean stress
σa_w	AM-component axial mean stress
σb	Bending-surface stress
σb_w	AM-component bending-surface stress

σ_i	AM design parameter standard deviation vector
ΔK	Stress-intensity-factor increment
ΔK_w	Stress-intensity-factor increment for AM-component
θ	Surface-crack stress-correction factor for elliptical integral
Φ	Cumulative standard normal distribution function
AM	Additive manufacturing
FORM	First-order reliability method
FEM	Finite-element method
FWMSV	Failure-weighted mean-square value
HYP	Hot Isostatic Pressure
PDF	Probability distribution function
POD	Probability of detection
SIF	Stress-intensity factor

References

1. Ivan Meneghin, I.; Ivetic, G.; Stiller, M.; Molinari, G.; Ristori, V.; Ratta, S.D.; Dumont, F. Fatigue in additive manufactured aircraft: The long way to make it fly. In *ICAF-2019 Structural Integrity in the Age of Additive Manufacturing*; Niepokolczycki, A., Komorowski, J., Eds.; Springer: Cham, Switzerland, 2019; pp. 16–30. [CrossRef]
2. Sing, S.L.; Wiria, F.E.; Yeong, W.Y. Selective laser melting of lattice structures: A statistical approach to manufacturability and mechanical behaviour. *Robot. Com-Int. Manuf.* **2018**, *49*, 170–180. [CrossRef]
3. Carlton, H.D.; Haboub, A.; Gallegos, G.F.; Parkinson, D.Y.; MacDowell, A.A. Damage evolution and failure mechanisms in additively manufactured stainless steel. *Mater. Sci. Eng.* **2016**, *651*, 406–414. [CrossRef]
4. Girardin, E.; Renghini, C.; Dyson, J.; Calbucci, V.; Moroncini, F.; Albertini, G. Characterization of porosity in a laser sintered MMCp using X-ray synchrotron phase contrast microtomography. *Master Sci. Appl.* **2011**, *2*, 1322–1330. [CrossRef]
5. Plessis, A.D.; Yadroitsev, I.; Yadroitsava, I.; Le Roux, S.G. X-ray microcomputed tomography in additive manufacturing: A review of the current technology and applications. *3D Print Addit. Manuf.* **2018**, *5*, 227–247. [CrossRef]
6. Pour, M.A.; Zanoni, S. Impact of merging components by additive manufacturing in spare parts management. *Proced. Manuf.* **2017**, *11*, 610–618. [CrossRef]
7. De Baere, D.; Strantza, M.; Hinderdael, M.; Devesse, W.; Guillaume, P. Effective structural health monitoring with additive manufacturing. In Proceedings of the 7th European Workshop on Structural Health Monitoring Conference, EWSHM, Nantes, France, 8–11 July 2014.
8. Cerniglia, D.; Montinaro, N. Defect detection in additively manufactured components: Laser ultrasound and laser thermography comparison. *Proced. Struct. Integr.* **2018**, *8*, 154–162. [CrossRef]
9. Ortega, N.; Martinez, S.; Cerrillo, I.; Lamikiz, A.; Ukar, E. Computed tomography approach to quality control of the Inconel 718 components obtained by additive manufacturing (SLM). *Proced. Manuf.* **2017**, *13*, 116–123. [CrossRef]
10. DebRoy, T.; Wei, H.L.; Zuback, J.S.; Mukherjee, T.; Elmer, J.W.; Milewski, J.O.; Beese, A.M.; Wilson-Heid, A.; De, A.; Zhang, W. Additive manufacturing of metallic components—Process, structure and properties. *Prog. Mater. Sci.* **2018**, *92*, 112–224. [CrossRef]
11. Mukherjee, T.; Zuback, J.S.; De, A.; DebRoy, T. Printability of alloys for additive manufacturing. *Sci. Rep. UK* **2016**, *6*, 1–6. [CrossRef]
12. Aboulkhaira, N.T.; Everitta, N.M.; Ashcroftb, I.; Tuckba, C. Reducing porosity in AlSi10Mg parts processed by selective laser melting. *Addit. Manuf.* **2014**, *1–4*, 77–86. [CrossRef]
13. Avilés, A.; Avilés, R.; Albizuri, J.; Pallarés-Santasmartas, L.; Rodríguez, A. Effect of shot-peening and low-plasticity burnishing on the high-cycle fatigue strength of DIN 34CrNiMo6 alloy steel. *Int. J. Fatigue* **2019**, *119*, 338–354. [CrossRef]
14. Ayesta, I.; Izquierdo, B.; Flaño, O.; Sánchez, J.; Albizuri, J.; Avilés, R. Influence of the WEDM process on the fatigue behavior of Inconel® 718. *Int. J. Fatigue* **2016**, *92*, 220–233. [CrossRef]
15. Avilés, R.; Albizuri, J.; Rodríguez, A.; López de Lacalle, L.N. On the fatigue strength of ball burnished mechanical elements. *Mech. Mach. Sci.* **2014**, *17*, 365–373. [CrossRef]

16. Afkhami, S.; Dabiri, M.; Habib Alavi, S.; Björk, T.; Salminen, A. Fatigue characteristics of steels manufactured by selective laser melting. *Int. J. Fatigue* **2019**, *122*, 72–83. [CrossRef]
17. Coro, A.; Abasolo, M.; Aguirrebeitia, J.; López de Lacalle, L.N. Inspection scheduling based on reliability updating of gas turbine welded structures. *Adv. Mech. Eng.* **2019**, *11*, 1–20. [CrossRef]
18. Kale, A.A.; Haftka, R.T. Tradeoff of weight and inspection cost in reliability-based structural optimization. *J. Aircr.* **2008**, *45*, 77–85. [CrossRef]
19. Opgenoord, M.J.; Willcox, K.E. Sensitivity analysis methods for uncertainty budgeting in system design. *AIAA J.* **2016**, *54*, 3134–3148. [CrossRef]
20. Millwater, H.R.; Wieland, D.H. Probabilistic sensitivity-based ranking of damage tolerance analysis elements. *J. Aircr.* **2010**, *47*, 161–171. [CrossRef]
21. Paris, P.; Erdogan, F. A critical analysis of crack propagation laws. *J. Basic Eng.* **1963**, *85*, 528–533. [CrossRef]
22. US Department of Transportation. *Damage Tolerance for High Energy Turbine Engine Rotors, Advisory Circular AC 33.14-1*; Federal Aviation Administration, US Department of Transportation: Washington, DC, USA, 2001.
23. Wu, Y.T.; Enright, M.P.; Millwater, H.R. Probabilistic methods for design assessment of reliability with inspection. *AIAA J.* **2002**, *40*, 937–946. [CrossRef]
24. Coppe, A.; Pais, M.J.; Haftka, R.T.; Kim, N.H. Using a simple crack growth model in predicting remaining useful life. *J. Aircr.* **2012**, *49*, 1965–1973. [CrossRef]
25. Thoft-Christensen, P.; Murotsu, Y. *Application of Structural Systems Reliability Theory*; Springer: Berlin, Germany, 1986.
26. Madsen, H.O.; Krenk, S.; Lind, N.C. *Methods of Structural Safety*; Dover Publications: New York, NY, USA, 2006.
27. Feng, G.Q.; Garbatov, Y.; Guedes Soares, C. Fatigue reliability of a stiffened panel subjected to correlated crack growth. *Struct. Saf.* **2011**, *36–37*, 39–46. [CrossRef]
28. Feng, G.Q.; Garbatov, Y.; Guedes Soares, C. Probabilistic model of the growth of correlated cracks in a stiffened panel. *Eng. Fract. Mech.* **2012**, *84*, 83–95. [CrossRef]
29. Kapur, K.R.; Lamberson, L.R. *Reliability in Engineering Design*; John Wiley & Sons: Hoboken, NJ, USA, 1977.
30. Kim, N.H.; Pattabhiraman, S.; Houck, L.A. Bayesian approach for fatigue life prediction from field data. *ASME* **2010**, *GT2010-23780*, 695–703.
31. Bhachu, K.S.; Haftka, R.T.; Waycaster, G.; Kim, N.H.; Hurst, C. Probabilistic manufacturing tolerance optimization of damage-tolerant aircraft structures using measured data. *J. Aircr.* **2015**, *52*, 1412–1421. [CrossRef]
32. López de Lacalle, L.N.; Viadero, F.; Hernández, J.M. Applications of dynamic measurements to structural reliability updating. *Probab. Eng. Mech.* **1996**, *11*, 97–105. [CrossRef]
33. Ditlevsen, O. *Uncertainty Modeling*; McGraw-Hill: New York, NY, USA, 1981.
34. Viadero, F.; Bueno, J.I.; López de Lacalle, L.N.; Sancibrián, R. Reliability computation on stiffened bending plates. *Adv. Eng. Softw.* **1995**, *20*, 43–48. [CrossRef]
35. MIL-HDBK-1823A. *Nondestructive Evaluation System Reliability*; Department of Defense: Washington, DC, USA, 2009.
36. ASTM E647. *Standard Test Method for Measurement of Fatigue Growth Rates*; ASTM International: West Conshohocken, PA, USA, 2015.
37. ASTM E1820. *Standard Test Method Measurement of Fracture Toughness*; ASTM International: West Conshohocken, PA, USA, 2018.
38. Daniewicz, S.R.; Collins, J.A.; Houser, D.R. An elastic-plastic analytical model for predicting fatigue crack growth in arbitrary edge-cracked two-dimensional geometries with residual stress. *Int. J. Fatigue* **1994**, *16*, 123–133. [CrossRef]
39. Maddox, S.J. *Fitness-for-Purpose Assessment of Misalignment in Transverse Butt Welds Subject to Fatigue Loading*; TWI Industrial Member Report; TWI Ltd.: Cambridge, UK, 1985.
40. Wilson, C.D. *Linear Elastic Fracture Mechanics Primer*; Technical Memorandum 103591; NASA: Washington, DC, USA, 1992.
41. Newman, J.C.; Raju, I.S. An empirical stress-intensity factor equation for the surface cracks. *Eng. Fract. Mech.* **1981**, *15*, 185–192. [CrossRef]
42. Sundararajan, C.R.; Hudak, B.Y. *Probabilistic Structural Mechanics Handbook: Theory and Industrial Applications*; Springer: New York, NY, USA, 1995; pp. 116–117.

43. Lee, Y.D.; McClung, R.C.; Chell, G.G. An efficient stress intensity factor solution scheme for corner cracks at holes under bivariant stressing. *Fatigue Fract. Eng. Mater. Struct.* **2008**, *31*, 1004–1016. [CrossRef]
44. Uslu, M.; Demir, O.; Ayhan, A.O. Surface cracks in finite thickness plates under thermal and displacement-controlled loads—Part 1: Stress intensity factors. *Eng. Fract. Mech.* **2014**, *115*, 284–295. [CrossRef]
45. Uslu, M.; Demir, O.; Ayhan, A.O. Surface cracks in finite thickness plates under thermal and displacement-controlled loads—Part 2: Crack propagation. *Eng. Fract. Mech.* **2014**, *115*, 255–269. [CrossRef]
46. FINET European Fitness-for-Service Network. *Selection of Failure Assessment Diagram Fracture Module. Fracture-Fatigue-Creep-Corrosion*; FITNET European Fitness-for-Service: Cambridge, UK, 2008; Volume 6.2.3.2.
47. Melchers, R.E. *Structural Reliability Analysis and Prediction*; Ellis Horwood Chichester: New York, NY, USA, 1987.
48. Smirnov, V. *A Course of Higher Mathematics*, 1st ed.; Adiwes International Series in Mathematics; Pergamon: Oxford, UK, 1964.
49. Ditlevsen, O.; Bjerager, P. Methods of structural systems reliability. *Struct. Saf.* **1986**, *3*, 195–229. [CrossRef]
50. Bjerager, P. On computation methods for structural reliability analysis. *Struct. Saf.* **1990**, *9*, 79–96. [CrossRef]
51. Hasofer, A.M.; Lind, N.C. Exact and invariant second-moment code format. *J. Eng. Mech.* **1974**, *100*, 111–121.
52. Low, B.K.; Wilson, H.; Tang, H. Reliability analysis using object-oriented constrained optimization. *Struct. Saf.* **2004**, *26*, 69–89. [CrossRef]
53. Fox, R.L. *Optimization Method and Engineering Design*; Method of Feasible Directions; Addison-Wesley Pub. Co.: Boston, MA, USA, 1971; pp. 179–195.
54. Hohenbichler, M.; Rackwitz, R. Sensitivity and importance measures in structural reliability. *J. Civil Eng. Syst.* **1986**, *3*, 203–206. [CrossRef]
55. Bjerager, P.; Krenk, S. Parametric sensitivity in first order reliability theory. *J. Eng. Mech.* **1989**, *115*, 1577–1582. [CrossRef]
56. US Department of Transportation. *Damage Tolerance of Hole Features in High-Energy Turbine Engine Rotor, Advisory Circular AC 33.70-2*; Federal Aviation Administration, US Department of Transportation: Washington, DC, USA, 2009.
57. Bean, G.B.; Witkin, D.B.; McLouth, T.D.; Patel, D.N.; Zaldivar, R.J. Effect of laser focus shift on surface quality and density of Inconel 718 parts produced via selective laser melting. *Addit. Manuf.* **2018**, *22*, 207–215. [CrossRef]
58. Plaskitt, R.; Halfpenny, A.; Hill, M. Strain controlled fatigue testing of additive manufactured titanium alloy Ti-6Al-4V. *ICAF 2019 Struct. Integr. Age Addit. Manuf.* **2019**, 43–55. [CrossRef]
59. Zhang, X.; Syed, A.K.; Biswal, R.; Martina, F.; Ding, J.; Williams, S. High cycle fatigue and fatigue crack growth rate in additive manufactured titanium alloys. *ICAF 2019 Struct. Integr. Age Addit. Manuf.* **2019**, 31–42. [CrossRef]